

## Acoustofluidic Chemical Waveform Generator and Switch

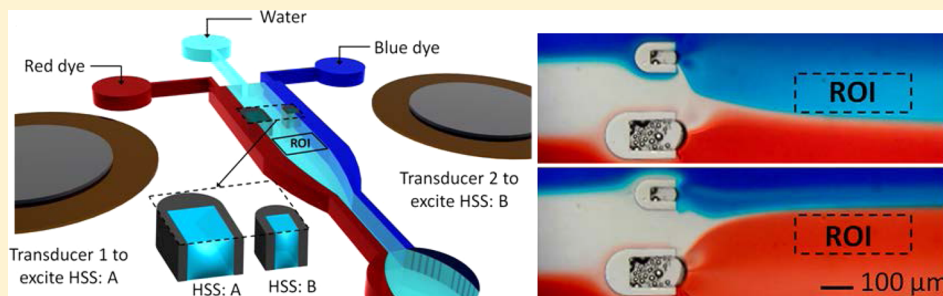
Daniel Ahmed,<sup>†</sup> Hari S. Muddana,<sup>‡</sup> Mengqian Lu,<sup>†</sup> Jarrod B. French,<sup>§</sup> Adem Ozcelik,<sup>†</sup> Ye Fang,<sup>||</sup> Peter J. Butler,<sup>‡</sup> Stephen J. Benkovic,<sup>§</sup> Andreas Manz,<sup>†</sup> and Tony Jun Huang<sup>\*,†</sup>

<sup>†</sup>Department of Engineering Science and Mechanics, <sup>‡</sup>Biomedical Engineering, <sup>§</sup>Department of Chemistry, The Pennsylvania State University, University Park, Pennsylvania 16802, United States

<sup>||</sup>Biochemical Technologies, Science and Technology Division, Corning Corporation, Corning, New York 14830, United States

<sup>†</sup>KIST Europe, Campus E 71, 66123 Saarbruecken, Germany

### Supporting Information



**ABSTRACT:** Eliciting a cellular response to a changing chemical microenvironment is central to many biological processes including gene expression, cell migration, differentiation, apoptosis, and intercellular signaling. The nature and scope of the response is highly dependent upon the spatiotemporal characteristics of the stimulus. To date, studies that investigate this phenomenon have been limited to digital (or step) chemical stimulation with little control over the temporal counterparts. Here, we demonstrate an acoustofluidic (i.e., fusion of acoustics and microfluidics) approach for generating programmable chemical waveforms that permits continuous modulation of the signal characteristics including the amplitude (i.e., sample concentration), shape, frequency, and duty cycle, with frequencies reaching up to 30 Hz. Furthermore, we show fast switching between multiple distinct stimuli, wherein the waveform of each stimulus is independently controlled. Using our device, we characterized the frequency-dependent activation and internalization of the  $\beta_2$ -adrenergic receptor ( $\beta_2$ -AR), a prototypic G-protein coupled receptor (GPCR), using epinephrine. The acoustofluidic-based programmable chemical waveform generation and switching method presented herein is expected to be a powerful tool for the investigation and characterization of the kinetics and other dynamic properties of many biological and biochemical processes.

Biochemical cues with identical chemical compositions can result in varied biological outcomes when given with different spatiotemporal characteristics.<sup>1,2</sup> Emulating the local microenvironment of the cell with high spatial and temporal fidelity provides researchers with important degrees of freedom when studying dynamic biological and biomolecular processes.<sup>3–9</sup> Microfluidics has been applied to such studies<sup>10–12</sup> because it offers a level of high-precision fluidic control<sup>13–15</sup> lacking in bulk systems. While progress has been made toward the spatial modulation of chemical stimuli in microfluidics through the generation of spatial chemical gradients,<sup>16–18</sup> temporal modulation has received limited attention. Techniques for temporal manipulation of chemical stimuli<sup>19–26</sup> are usually based on the concept of switching between two or more liquid inlets,<sup>10,22,26,27</sup> analogous to a multiplexer in electronics. These designs require sophisticated fabrication methods (numerous external moving parts),<sup>26–28</sup> exotic materials,<sup>19,20,23</sup> and/or have slow temporal responses (working frequencies limited to 1 Hz).<sup>27</sup> In addition, although digital (i.e., step stimuli) waveforms are generated conveniently,

continuous modulation of the amplitude and/or frequency (i.e., analog waveforms) has been difficult.<sup>29</sup>

Here, we demonstrate that a bubble oscillating in an acoustic field provides a unique and versatile method to generate arbitrary temporal chemical waveforms. This work is built upon our previous findings that acoustically oscillating bubbles can effectively mix fluids in a microfluidic channel.<sup>30–32</sup> Compared with existing micromixers,<sup>33–40</sup> our acoustic bubble-based micromixer seems to be more suitable for chemical waveform and switch generation because it enables fast mixing time, can be turned on and off instantaneously, and can be spatially predesigned anywhere within the microfluidic channel (with the advent of horseshoe structure). In addition, multiple acoustic bubble-based micromixers can work independently within the microfluidic channel. Our approach is capable of

**Received:** September 7, 2014

**Accepted:** November 5, 2014

**Published:** November 18, 2014

generating not only digital chemical waveforms but also analog waveforms (arbitrary stimuli) whose characteristics, including shape, frequency, amplitude, and duty cycle, can be conveniently modulated. Furthermore, by trapping multiple bubbles in a single microchannel, we demonstrate switching between two distinct stimuli, wherein the waveform of each stimulus can be independently controlled. To demonstrate the capability of our device to characterize fast biological processes, we show that the temporal response of epinephrine-induced activation and subsequent internalization of  $\beta_2$ -adrenergic receptor ( $\beta_2$ -AR), a prototypic G-protein coupled receptor (GPCR), can be monitored in live cells by precisely controlling the duration of stimulation.

## EXPERIMENTS

**Device Fabrication.** A single-layer PDMS microchannel was fabricated using the soft lithography and the mold replica technique.<sup>30–32</sup> In short, a silicon mold for the microchannel was patterned in photoresist (Shipley 1827, MicroChem) and etched with deep reactive ion etching (DRIE). The mold was then coated with 1H,1H,2H,2H-perfluorooctyl-trichlorosilane (Sigma-Aldrich) to reduce its surface energy and any subsequent damage to the PDMS channel during the demolding process. SylgardTM 184 silicone elastomer base and SylgardTM 184 silicone elastomer curing agent (Dow Corning) were mixed at a 10:1 weight ratio and cast onto the silicon mold. The uncured PDMS on the silicon mold was then degassed in a vacuum chamber for 2 h to remove any air bubbles and later cured at 65 °C for 45 min. After removing the cured PDMS from the mold, the inlets and the outlets were drilled into the PDMS using a silicon carbide drill bit (model 220/395, Dremel). The microfluidic channel was then bonded to a microcover glass, which had been pretreated with oxygen plasma. A piezoelectric transducer (model no. 273-073, RadioShack) was then attached to the glass slide adjacent to the channel using epoxy (Permatex 84101).

**Experimental Details.** The glass slide, including the microfluidic channel and the piezoelectric transducer, was mounted on a Nikon TE-2000U optical microscope stage. Ink (PAR3001100, Parker) or food dye (Assorted/NEON, McCormick) was infused into the channel through a 1 mL syringe (Becton Dickinson) by automated syringe pumps (KDS Legato 210). Once the bubbles were stably trapped with a smooth flow, the transducer was connected to a function generator to control the bubble activation/deactivation via a function generator (HP8116A/Tektronix AFG 3011). The driving voltages used in the experiments were 8–16 V<sub>pp</sub>.

**Data/Image Acquisition and Analysis.** Data acquisition for the waveform generation was directly achieved by region of interest (ROI) selection during the experiment using InVivo (MediaCybernetics) microscopy software, connected to a CoolSnap HQ2 (Photometrics) CCD camera. The images in Figure 3 were captured at 1200 fps (to record the fast dynamics of each stimulus) and later processed through a home-built Matlab code. The remaining waveform and switching images were captured by Nikon D3S or Coolsnap CCD cameras. All movies were captured by a Nikon D3S or Casio EX-F1. Raw movie files were encoded into a stack of images and further processed using ImageJ software.

**Cell Line and Culture.** A HEK293 cell line that was stably transfected with human  $\beta_2$ -AR-GFP was established at Corning Inc. (Corning, NY). Briefly, HEK293 cells were transfected with pCMV- $\beta_2$ AR-GFP (OriGene, Rockville, MD) using

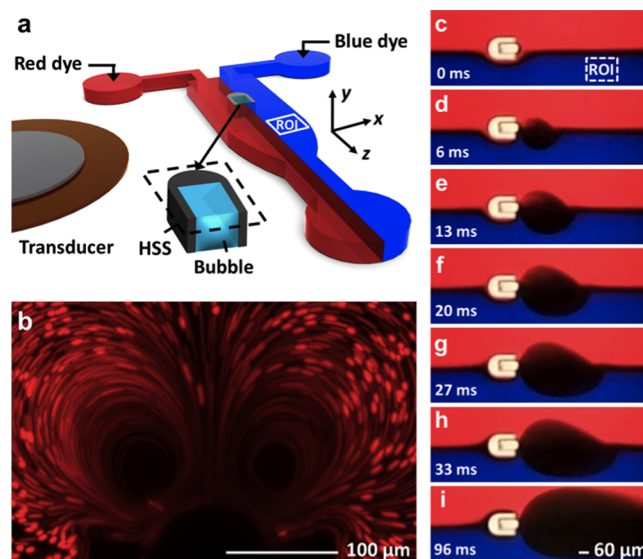


**Figure 1.** Concept of waveform generation. (a) Schematic of the experimental setup (see the Supporting Information for experimental details). The piezoelectric transducer, which generates low-intensity acoustic waves, is placed adjacent to the microfluidic channel on a glass slide. The acoustic waves drive the bubble trapped in the horseshoe structure (HSS), which is placed at the interface of the co-flowing liquids. (b) Experimental observation of acoustic microstreaming and flow recirculation during the bubble oscillation. (c–i) Mixing of red and blue dyes captured with high-speed imaging. The region of interest (ROI) for the output waveform was chosen ~300  $\mu\text{m}$  downstream of the HSS, in the bottom half of the channel. The chemical waveforms were determined by the optical density of the ROI when ink and buffer solutions were used.

Lipofectamine LTX Plus Reagent (Invitrogen) in a 6-well cell culture plate. The cells were treated with 500  $\mu\text{g}/\text{mL}$  G418 (Invitrogen) the next day. After transfection for 7 days, the surviving cells were diluted to 2–3 cells/well in a 96-well cell culture plate to allow the growth of clones derived from single cells. Stable clones with homogeneous expression level of  $\beta_2$ AR-GFP were selected by visualizing the GFP signal under a fluorescence microscope. The function of the GFP-tagged  $\beta_2$ -ARs were confirmed using receptor internalization and dynamics mass redistribution assay (see also Supporting Information Figure S7). These stable cell lines were maintained in DMEM containing 10% FBS, penicillin/streptomycin, L-glutamine, and 500  $\mu\text{g}/\text{mL}$  G418. Prior to running the experiments, cells were trypsinized, and suspended cells were centrifuged at 800 rpm for 3 min. Cells were resuspended in 200–400  $\mu\text{L}$  MEM before incubation in microfluidic channels.

**Cell Culture in Microfluidics.** Microfluidic channels were coated with fibronectin (BD Biosciences) (0.1 mg/mL) for 1 h. Subsequently, the channels were washed by PBS several times. Ten million cells/mL were suspended in MEM solution and injected into the microfluidic channel. The cells were allowed to adhere inside the channel by 60–90 min of incubation. The stimulant (epinephrine, 10  $\mu\text{M}$ ) and buffer (culture medium) were injected at 1  $\mu\text{L}/\text{min}$  into the channel via a pump. Different stimuli lengths (duty cycle) are appropriately controlled by timing the ON and OFF states of the bubble oscillation. Internalization signals were then observed by fluorescence imaging.

**Fluorescence Microscopy of Living Cells.** Fluorescent images were captured using laser scanning confocal microscopy

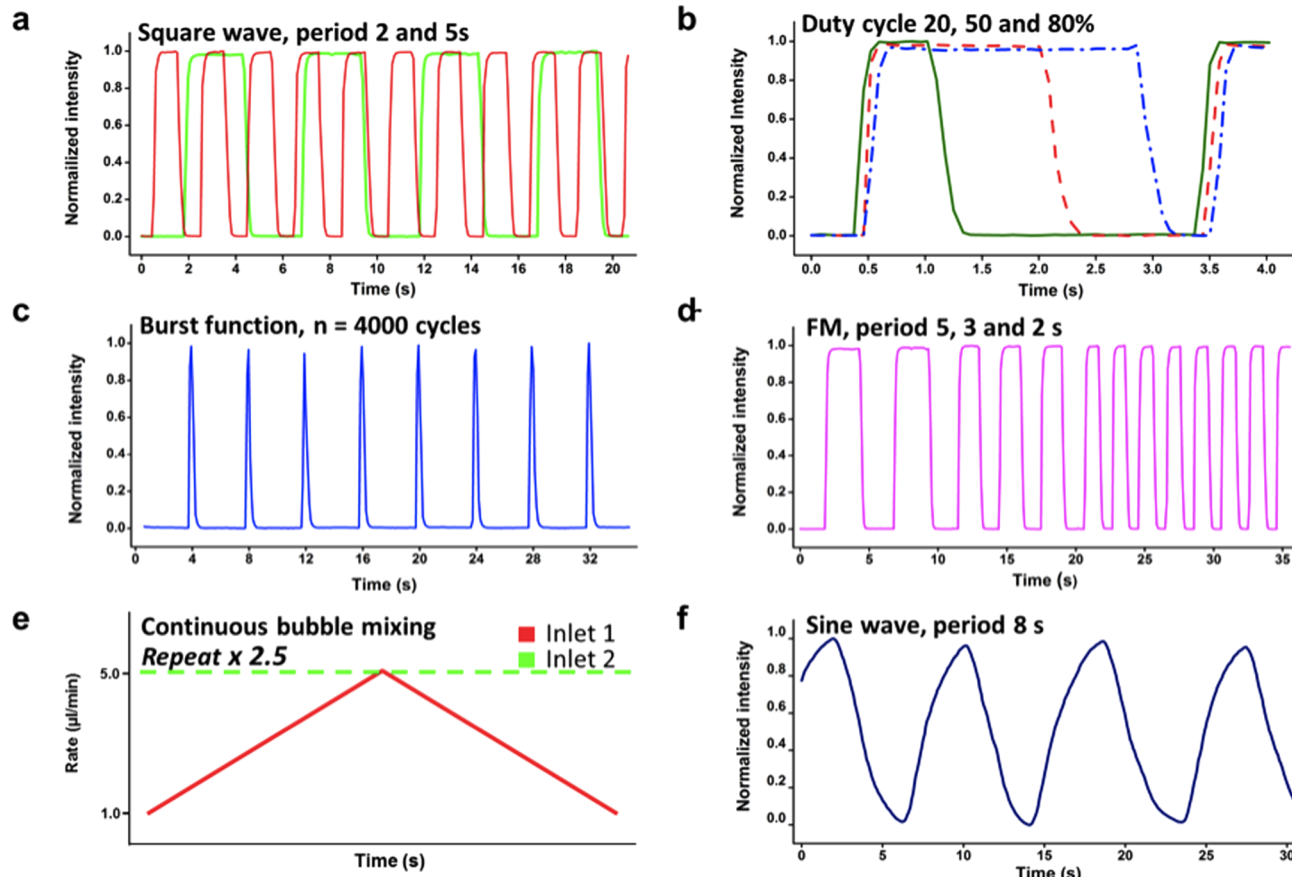


**Figure 2.** Generation of various chemical waveforms in the ROI marked in Figure 1c: (a) square wave, (b) duty cycle (green, 20%; red, 50%; and blue, 80%), (c) burst mode, (d) tunable frequency, (e) flow rate utilized using automated syringe pumps in achieving amplitude modulation, (f) sine wave (concentration modulation).

(Olympus FV300) with a 60 $\times$  objective (1.49 NA) at room temperature ( $\sim 25^\circ\text{C}$ ). Images were captured by FluoView 300 (version 4.3b). Cell imaging under microfluidics were captured by Nikon Eclipse TE 2000-U with a 20 $\times$  objective (0.45 NA) at room temperature ( $\sim 25^\circ\text{C}$ ). Images were captured by Nikon imaging software (NIS-Advanced) connected to a Hammatsu digital camera (C1140).

## RESULTS AND DISCUSSION

**Chemical Waveform Generator using Acoustically Activated Bubbles.** Figure 1a illustrates the schematic diagram of our acoustofluidic chemical waveform generator. A horseshoe structure (HSS) (see also Supporting Information Figure S1) inside a poly(dimethylsiloxane) (PDMS) microfluidic channel is used to trap a single bubble through surface tension (see Supporting Information Movies 1 and 2); the structure also helps to determine the size of the bubble. When driven by an adjacent piezoelectric transducer controlled by an electronic function generator, the membrane of the trapped bubble oscillates. The maximum oscillation of the bubble is achieved at its resonance frequency, which is size-dependent. At the resonance frequency, the second-order effect of the nonlinearity in the Navier–Stokes equation becomes prominent, giving rise to a pressure gradient in the fluid that drives the recirculating flow regions, commonly referred to as acoustic microstreaming,<sup>41,42,44–84</sup> depicted in Figure 1b.

When the trapped bubble is excited, the counter-rotating vortices resulting from microstreaming disrupt the clean

liquid–liquid interface in a manner that is characteristic of the laminar flow regime in the microchannel. The vortices drastically enhance the mass transport along the direction perpendicular to the flow, effectively mixing the inlet solutions. This is referred to as the ON state. This mixing process was observed using fast imaging (1200 frames/s) and is shown in Figure 1c–i and Supporting Information Movie 3. Complete mixing of the fluids occurred in less than 30 ms. When the acoustic field is turned off, the mixing stopped, and the characteristic laminar flow returned. This is referred to as the OFF state. The fast responses of the electric and acoustic systems allowed us to directly transform electrical signals into chemical waveforms, effectively implementing all the capacities of a function generator.

**Generation of Digital Chemical Waveforms.** To demonstrate the device's functionality, we generated a variety of different chemical waveforms (Figure 2a–d) using a function generator to control the acoustic excitation (see also Supporting Information Figure S4). In these experiments, we infused the two inlets with dye and a buffer solution at identical flow rates (6  $\mu\text{L}/\text{min}$ ). The ROI for the output waveform was chosen  $\sim 300 \mu\text{m}$  downstream of the HSS (i.e., past the recirculation zone), such that the stress developed by an oscillating bubble on cells under investigation is negligible.<sup>45</sup> The width of the ROI was chosen such that it falls within the mixing distance in the buffer region, whereas the length of ROI was arbitrarily chosen to fit at least 2–3 adherent cells under investigation. The optical density of a specified ROI was

used to determine the mixing efficiency and to give a rough estimate of the stimulant concentration, which was measured in greyscale values (estimated by ImageJ software). A square waveform was generated by simply switching the transducer on and off. The frequency (Figure 2a) and duty cycle (Figure 2b) of the signals were controlled by appropriately timing the ON and OFF states of the bubble oscillation. Burst/pulse signals were generated (Figure 2c) by lowering the transducer excitation duration to less than the complete mixing time (30 ms). We also show that the frequency of the chemical signal can be modulated without interruption (Figure 2d), with the potential for a continuous frequency sweep.

**Generation of Analog Chemical Waveforms.** In Figure 2a–d, we show several chemical waveforms with constant maximum and minimum amplitudes (digital waveforms). To generate analog signals, such as sinusoidal or triangular waveforms, it is essential to dynamically vary the amplitude of the stimulus (i.e., the concentration of the stimulus). This amplitude modulation was attained by continuously mixing the stimulus and buffer solutions while changing the relative flow rates of the inlets. The input flow rates applied to the microfluidic channel was manipulated by a computer-controlled syringe pump, as shown in Figure 2e. As the relative flow rates change between two fluids in a microchannel, the location of their interface shifts along the width of the channel due to the difference in inlet pressures (see Supporting Information Figure S5). This controllable interface can be used to vary the proportion of each fluid that is mixed by the bubble, resulting in a tunable output concentration of the stimulus. For example, a sine chemical waveform was achieved (Figure 2f). We note, however, that the amplitude modulation frequency is limited by the slow response (approximately second time-scale) of the flow pump. To achieve rapid amplitude modulation, independent of the pump response, we designed a three-inlet channel with a HSS at the center. The stimulus (ink) was injected in the center at a fixed flow rate of  $1 \mu\text{L}/\text{min}$ , whereas the buffers (water) were infused through the other inlets at a fixed flow rate of  $2.5 \mu\text{L}/\text{min}$  (Figure 3a). The trapped bubble was excited close to its resonance frequency, and the amplitude of oscillation, which scales linearly with the applied voltage, was tuned by the function generator.<sup>43</sup> As the voltage is increased, the mixing distance,  $d$ , of ink and water increases in a linear fashion. Figure 3b shows the step decrease in the stimulant concentration for a step increase of the voltage applied to the transducer in the selected ROI marked in Figure 3a. Note that the voltage can be tuned using smaller steps to achieve finer amplitude modulation. The ink concentration decreases because more buffer solution is mixed for a fixed volume of the stimulant. The change in concentration was attained almost instantaneously (inset of Figure 3b), which allowed us to tune the desired concentration. This concept can be readily used for applications that require rapid mixing and fine temporal control over stimulant concentrations such as single-shot chemical kinetics studies.<sup>55,56</sup>

**High-Frequency Characterization.** The digital frequency response of our device is intrinsically limited by the mixing capabilities of the bubble, properties of the fluids (e.g., density and surface tension), flow velocity, and location of the ROI. To quantify the high-frequency response of the device, we compared the photointensity of the ROI during partial mixing (pulse width less than the total mixing time) to the intensity at complete mixing to obtain a quantitative measure of the total mixing efficiency. Figure 4 shows the relative intensity,

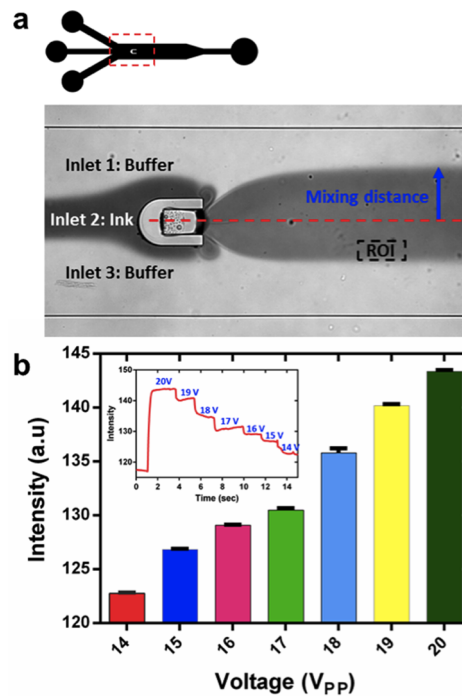


**Figure 3.** Rapid amplitude (concentration) modulation. (a) Schematic of the experimental setup for rapid amplitude modulation. The channel consists of a single HSS with three inlets and one outlet: inlets 1 and 3 were infused with a buffer solution (water), and inlet 2 was infused with stimuli (ink). When the bubble was acoustically activated, ink mixes with water with a mixing distance,  $d$ . (b) Graph shows dilution of the ink for increasing voltage in the selected ROI marked in panel a. The inset shows the raw amplitude modulation data, suggesting rapid modulation (less than 100 ms).

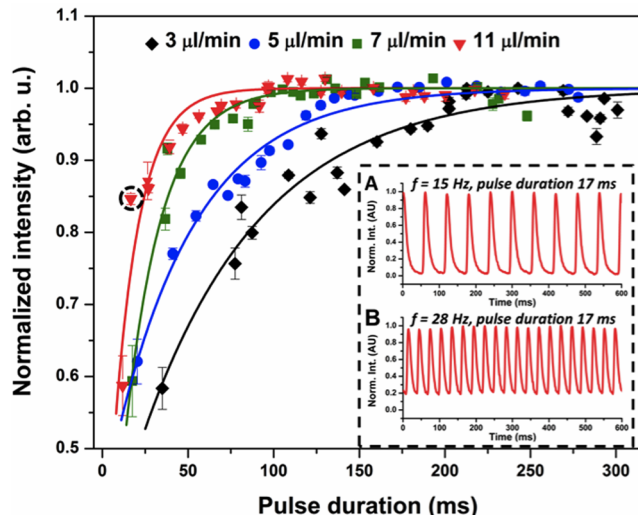


**Figure 4.** Characterization of frequency response. Frequency response of waveform generation with flow rates of 3, 5, 7, and  $11 \mu\text{L}/\text{min}$ . (Inset) Waveform generation utilizing 17 ms pulse duration (marked as dotted circle) at  $11 \mu\text{L}/\text{min}$  flow rate. (a) 15 Hz for 60 ms trigger interval; (b) 28 Hz for 30 ms trigger interval. Error bars represent the standard deviation from a minimum of five measurements.

indicative of mixing efficiency, at increasing pulse width duration for four different flow rates; the observed response is typical of a low-pass filter, where low frequencies show distinct chemical signals, but higher frequencies blur into a con-

tinuum. As seen in the inset of Figure 4a,b, the demixing time (i.e., the falling time), which is dependent on the flow rate, is the rate-limiting factor in the device's frequency response. Despite partial mixing, distinct chemical pulses can be generated at frequencies greater than 30 Hz, more than an order of magnitude faster than previous microfluidic designs ( $\sim 1$  Hz).<sup>27</sup>

**Chemical Switching using Multiple Bubbles.** While the generation of single chemical waveforms is vital to a variety of biochemical studies, dynamically switching between or concurrently applying different chemical stimuli can be useful to study more complex dynamic systems, such as cell signaling pathways<sup>57</sup> or cascades of biochemical reactions.<sup>58,59</sup> In principle, these studies require logic-type control utilizing multiple waveform generators. Independently mixing multiple waveforms within a single microchannel requires multiple trapped bubbles with different resonance frequencies so they may be excited separately. The resonance frequency of a bubble is governed by its geometry (i.e., radius) and the properties of the liquid. Assuming a constant liquid medium, we used HSS geometry to effectively alter the fundamental resonance frequency of the bubbles. Preventing cross-excitation due to higher-order harmonic modes of oscillation was the main challenge. We prescreened nine HSS geometries that varied in width (see Supporting Information Figures S2 and S6a). To determine the resonance frequency of each bubble, we swept

the excitation frequency from 10 to 60 kHz in 100 Hz increments while visually monitoring the oscillation amplitude for a distinct peak. The results are shown in Supporting Information Figure S6b.

Figure 5a shows a schematic diagram of the device used for switching between two different chemical signals. The channel has three inlets and one outlet: inlets 1 and 3 (peripheral regions) were infused with different chemical signals (red and blue dyes for demonstration), and inlet 2 pumped a buffer solution (water) into the central region that served as our ROI. Distinct HSSs ( $60 \times 90 \mu\text{m}$  and  $110 \times 165 \mu\text{m}$ ) were positioned at each liquid–liquid interface; the corresponding bubbles had resonant frequencies of 29.5 and 14.7 kHz (Figure 5a). Cross-excitation of the bubbles at the above frequencies was negligible, shown by the microstreaming bead test captured in Figure 5b. Figure 5c lays out the binary chemical circuitry: when bubble A was activated at  $f = 14.7$  kHz, only the red dye mixed with the water to fill the ROI (Figure 5d, bottom panel, and Supporting Information Movie 4). Conversely, when bubble B was activated at  $f = 29.5$  kHz, only the blue dye mixed with the water (Figure 5d, top panel, and Supporting Information Movie 5). Switching between the red and blue dyes was achieved by alternating between the two excitation frequencies (Figure 5e; see also Supporting Information Movie 6). This direct conversion of electrical

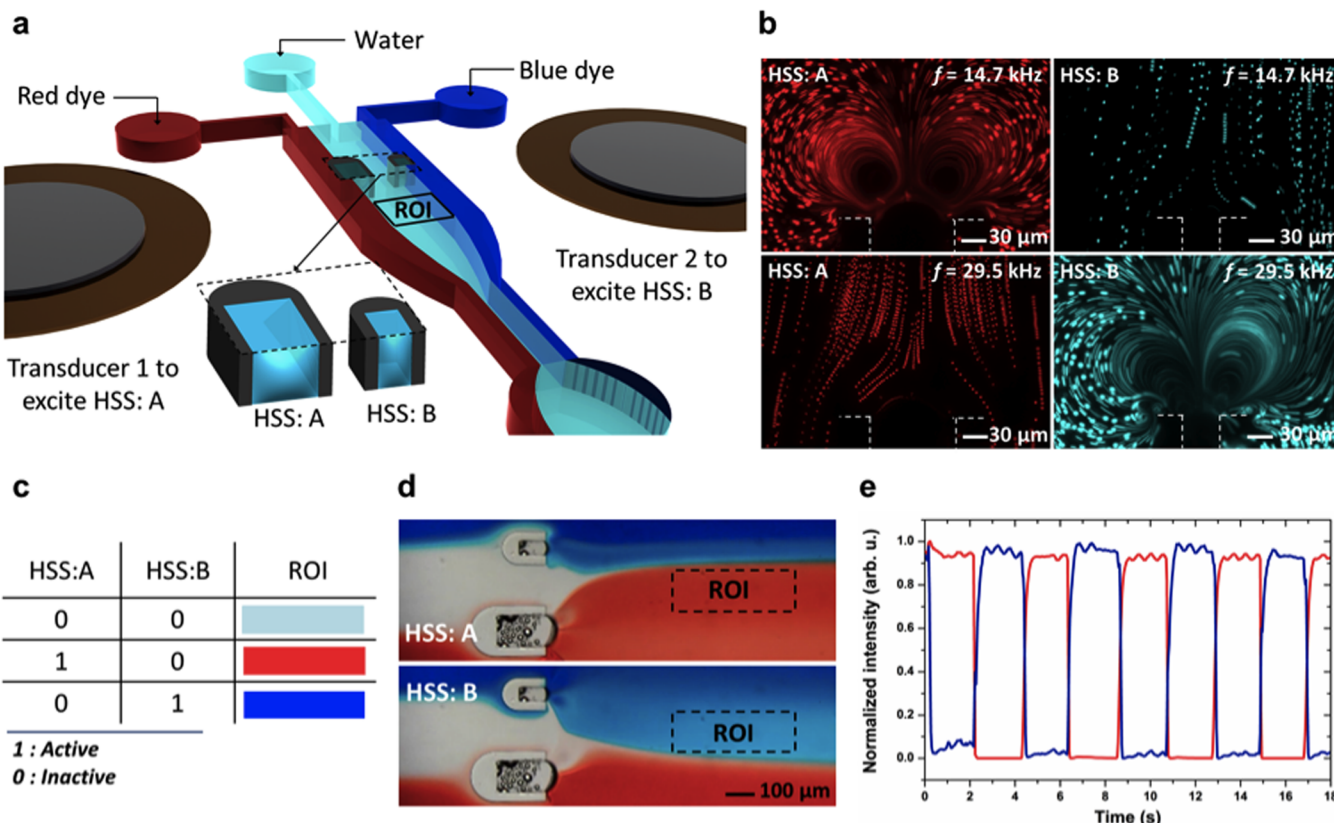


**Figure 5.** Bubble-based switching between multiple stimuli. (a) Schematic of the experimental setup for chemical switching. The microfluidic channel contains HSSs of different sizes and, subsequently, bubbles of different sizes that are independently driven by transducers bonded to the substrate adjacent to the channel. (b) Top, visualization of microstreaming from the bubble trapped in HSS A (red) while no streaming is observed in the bubble trapped in HSS B (blue) at an excitation frequency of 14.7 kHz. Bottom, visualization of the microstreaming from the bubble trapped in HSS B while no streaming occurs in HSS A at an excitation frequency of 29.5 kHz. (c) Table showing the concept of binary logic circuitry. (d) Results demonstrating switching between the blue and red dyes (see Supporting Information Movie 6 for further illustration). (e) Graph of experimental data for switching between red and blue dyes in the selected ROI marked in panel d.

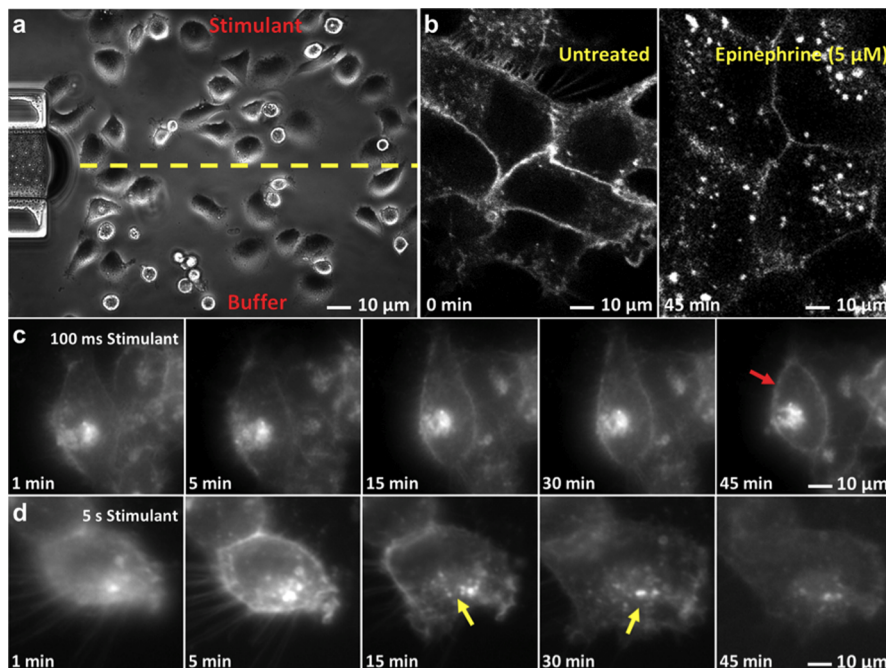


**Figure 6.** Temporal response of GPCR internalization using a chemical waveform. (a) Setup of chemical switching. A human embryonic kidney (HEK) 293 cell line that was stably transfected with a GFP-tagged  $\beta_2$ -AR was cultured inside the microfluidic waveform chip (see the Supporting Information for the experimental details). The stimulant (epinephrine, 10  $\mu$ M) and buffer (culture medium) are injected at 1  $\mu$ L/min into the channel. (b) GPCR internalization upon stimulation by 5  $\mu$ M epinephrine. Image taken at 45 min, demonstrating internalization (note that experiments were performed in Petri dishes). (c) No internalization of the labeled GPCR was observed in the microfluidic chip at a pulse width of 100 ms stimulant (red arrow indicates that the fluorescently labeled GPCRs remain unchanged at the membrane boundary). (d) Internalization of the labeled GPCR was observed in the microfluidic chip at a pulse width of 5 s of epinephrine (yellow arrow indicates internalization with an onset time of 15 min).

signals into chemical waveforms allows this device to access all of the previously demonstrated functions of the waveform generator, including frequency and amplitude modulation.

**GPCR Activation and Internalization.** To demonstrate the applicability of our device for studying dynamic biomolecular processes, we characterized the agonist-directed temporal desensitization of  $\beta_2$ -AR and the subsequent receptor internalization induced by epinephrine binding. GPCRs play an essential role in cellular homeostasis by binding external stimuli and initiating transduction pathways that lead to cellular responses. Upon prolonged or repeated exposure to agonists, GPCRs may become desensitized and internalized in clathrin-coated pits.<sup>60–63</sup> We monitored this process using a stably transfected cell line expressing GFP-tagged  $\beta_2$ -AR. The experimental setup is shown in Figure 6a, wherein a single trapped bubble is used to generate a temporally controlled pulse of chemical stimulant, epinephrine (5  $\mu$ M), over a culture of human embryonic kidney (HEK) cells (see the Supporting Information for further experimental details). Without treatment, the GFP fluorescence is predominantly located at the cell plasma membrane (Figure 6b). Upon continuous treatment with epinephrine for 45 min, GFP-tagged  $\beta_2$ -ARs are translocated from the plasma membrane surface to the cell interior, as indicated by the decreased fluorescence at the cell boundary and the increase in  $\beta_2$ -AR-loaded endosomes (Figure 6b). A punctate staining pattern within the cytoplasm, arising from endosomes containing the GFP-tagged  $\beta_2$ -AR, was used as the means to infer whether the applied pulse of epinephrine led to  $\beta_2$ -AR activation and internalization. When the stimulant pulse was applied for a duration of 100 ms, no significant internalization of  $\beta_2$ -ARs was observed, as shown in the time

series of Figure 6c. Even after 45 min, the fluorescently labeled  $\beta_2$ -ARs are largely observed at the membrane boundary, with no significant increase in labeled endosomes in the cell interior. Conversely, when the stimulant pulse was applied for a duration of 5 s, significant internalization of  $\beta_2$ -ARs takes place (Figure 6d) with an onset time of 15 min. This result is significant in that an agonist stimulation duration as short as 5 s is sufficient to cause receptor internalization. Epinephrine is an endogenous agonist for the  $\beta_2$ -AR with rapid on and off rates, and its residence time (reciprocal to the off rate) to the  $\beta_2$ -AR is estimated to be less than 0.2 s.<sup>64</sup> However, the agonist-stimulated  $\beta_2$ -AR internalization in HEK cells is dependent on phosphorylation of the agonist-stimulated receptor by G-protein-coupled receptor kinase 2 (GRK2) followed by binding of  $\beta$ -arrestins to the phosphorylated receptor,<sup>65,66</sup> and it requires persistent agonist occupancy.<sup>66,67</sup> The GRK-dependent phosphorylation is the rate-limiting step in the receptor internalization and often takes several minutes for completion.<sup>66,68</sup> Our result clearly demonstrates the temporal nature of  $\beta_2$ -AR activation and internalization due to epinephrine binding in cells, a result that would be difficult to demonstrate in cells using conventional techniques (e.g., single-molecule fluorescence spectroscopy). Given that most signaling events take place with different spatial–temporal dynamics, our acoustofluidic<sup>69–72</sup> system offers a promising tool for controlling and characterizing the dynamics of biomolecular processes in the native cellular context.

## CONCLUSIONS

Chemical waveforms, when compared to constant chemical signals, can have markedly different effects on cellular signaling

pathways that receive, transmit, process, and implement directions from chemical stimuli. With the on-chip waveform generator and switch reported here, it is possible to study the dynamics of receptor-mediated signaling and other cellular responses under well-defined chemical microenvironments, an important step to understand *in vivo* receptor biology and drug action. A constant challenge when studying biological phenomenon in cells is the variability encountered in samples and conditions. The chemical composition of the medium in which cell cultures are maintained is, by nature, complex and constantly undergoing change. As a result, comparisons between replicate samples of cells grown under otherwise similar experimental conditions can be confounded by batch-to-batch variations in media composition and environmental conditions.

Using the technology described herein, it is possible to expose cells within the same culture to different stimuli while maintaining the temperature, pH, and other growth conditions at precisely the same values for all components of the system. In this way, rigorous experimental controls can be carried out alongside the measurements of interest with certainty that all samples will experience the same conditions. This method also provides a powerful tool for the study of signal transmission and intercellular communication. By carefully controlling the shape of the chemical waveform administered to a sample, a subset of the population can be treated with a stimulant while the remainder of the population is left untreated. This enables the *in situ* investigation of signal transmission or communication without the need to physically isolate or manipulate the cells. Another significant benefit of this technology is the ability to temporally control the chemical waveforms generated. This makes possible the measurement of biological phenomena that span a broad range of time scales and enables the measurement of the kinetics of these processes. Applications where these features are of particular use include the investigation of fast cellular signaling events and the characterization of pharmacokinetics at the single-cell level.<sup>73</sup> Finally, generating waveforms in continuous flow also eliminates the abrupt changes in shear stress at the cell membrane that occur in segmented flow devices, more closely mimicking *in vivo* chemical signals. The capability of this device to generate temporally controlled analog waveforms in controlled environments is expected to be of significant benefit to those studying myriad cellular phenomena and is sure to find applications in the investigation and characterization of intercellular signaling, cancer metastasis, immunochemistry, stem cell differentiation, and many other cellular events that require precise spatial and temporal control over local chemical environments.

## ASSOCIATED CONTENT

### Supporting Information

Figure S1: Two images of the horseshoe structure (HSS). Figure S2: 3 × 3 array of HSS used to prescreen the appropriate dimensions of the two HSSs that were later utilized in the chemical switching device. Figure S3: Design and dimensions of the microchannels used for chemical waveform generation and switching. Figure S4: Electrical signals applied to the piezoelectric transducer by the function generator driving at the resonance frequency of the bubble. Figure S5: Image sequence showing the shift of the interface by the flow rate applied in Figure 2e but with no mixing. Figure S6: Characterization of bubbles' resonance frequencies. Figure S7: DMR characterization of the  $\beta_2$ -ARs. Table S1: Optimized flow rates for

repeatable bubble traps within the HSS. Movie S1: Single bubble trap. Movie S2: Multiple bubble traps. Movie S3: Mixing of red and blue food dye. Movie S4: Larger bubble excitation. Movie S5: Smaller bubble excitation. Movie S6: Chemical binary switch. This material is available free of charge via the Internet at <http://pubs.acs.org>.

## AUTHOR INFORMATION

### Corresponding Author

\*Tel.: 814-863-4209; Fax: 814-865-9974; E-mail: junhuang@psu.edu.

### Notes

The authors declare no competing financial interest.

## ACKNOWLEDGMENTS

This research was supported by the National Institutes of Health (1 R01 GM112048-01A1 and 1R33EB019785-01), the National Science Foundation (CBET-1438126 and IIP-1346440), and the Penn State Center for Nanoscale Science (MRSEC) under grant DMR-0820404. Components of this work were conducted at the Penn State node of the NSF-funded National Nanotechnology Infrastructure Network. The authors thank Peng Li, Chung Yu Chan, and Michael Ian Lapsley for helpful discussions.

## REFERENCES

- (1) Shimizu, T. S.; Tu, Y.; Berg, H. C. *Mol. Syst. Biol.* **2010**, *6*, 382.
- (2) Lipan, O.; Wong, W. H. *Proc. Natl. Acad. Sci. U.S.A.* **2005**, *102*, 7063–7068.
- (3) Ghafar-zadeh, E.; Waldeisen, R.; Lee, L. P. *Lab Chip* **2011**, *11*, 3031–3048.
- (4) Wlodkowic, D.; Skommer, J.; Faley, S.; Darzynkiewicz, Z.; Cooper, J. M. *Exp. Cell Res.* **2009**, *315*, 1706–1714.
- (5) Park, J.; Kim, S.; Park, S. I.; Choe, Y.; Li, J.; Han, A. *J. Neurosci. Methods* **2014**, *221*, 166–174.
- (6) Issadore, D.; Franke, T.; Brown, K. A.; Westervelt, R. M. *Lab Chip* **2010**, *10*, 2937–2943.
- (7) Gurkan, U. A.; Tasoglu, S.; Akkaynak, D.; Avci, O.; Unluisler, S.; Canikyan, S.; Macallum, N.; Demirci, U. *Adv. Healthcare Mater.* **2012**, *1*, 661–668.
- (8) Wu, Y.; Buranda, T.; Simons, P. C.; Lopez, G. P.; McIntire, W. E.; Garrison, J. C.; Prossnitz, E. R.; Sklar, L. A. *Anal. Biochem.* **2007**, *371*, 10–20.
- (9) Ghoorjian, A.; Chilkoti, A.; López, G. P. *Anal. Chem.* **2014**, *86*, 6103–6110.
- (10) Hersen, P.; McClean, M. N.; Mahadevan, L.; Ramanathan, S. *Proc. Natl. Acad. Sci. U.S.A.* **2008**, *105*, 7165–7170.
- (11) Meier, B.; Zielinski, A.; Weber, C.; Arcizet, D.; Youssef, S.; Franosch, T.; Rädler, J. O.; Heinrich, D. *Proc. Natl. Acad. Sci. U.S.A.* **2011**, *108*, 11417–11422.
- (12) Gurkan, U. A.; Anand, T.; Tas, H.; Elkan, D.; Akay, A.; Keles, H. O.; Demirci, U. *Lab Chip* **2011**, *11*, 3979–3989.
- (13) Yang, Y.; Liu, a Q.; Chin, L. K.; Zhang, X. M.; Tsai, D. P.; Lin, C. L.; Lu, C.; Wang, G. P.; Zheludev, N. I. *Nat. Commun.* **2012**, *3*, 651.
- (14) Park, J.; Wu, J.; Polymenis, M.; Han, A. *Lab Chip* **2013**, *13*, 4217–4224.
- (15) Franke, T. A.; Wixforth, A. *ChemPhysChem* **2008**, *9*, 2140–2156.
- (16) Berthier, E.; Surfus, J.; Verbsky, J.; Beebe, D. *Integr. Biol.* **2010**, *2*, 630–638.
- (17) Keenan, T. M.; Folch, A. *Lab Chip* **2008**, *8*, 34–57.
- (18) Irimia, D.; Geba, D. A.; Toner, M. *Anal. Chem.* **2006**, *78*, 3472–3477.
- (19) Goulpeau, J.; Lonetti, B.; Trouchet, D.; Ajdari, A.; Tabeling, P. *Lab Chip* **2007**, *7*, 1154–1161.

- (20) Bae, A. J.; Beta, C.; Bodenschatz, E. *Lab Chip* **2009**, *9*, 3059–3065.
- (21) Eriksson, E.; Scott, K.; Lundqvist, F.; Svenningsson, M.; Scrimgeour, J.; Hanstorp, D.; Goksor, M.; Graneli, A. *Lab Chip* **2010**, *10*, 617–625.
- (22) Olofsson, J.; Bridle, H.; Sinclair, J.; Granfeldt, D.; Sahlin, E.; Orwar, O. *Proc. Natl. Acad. Sci. U.S.A.* **2005**, *102*, 8097–8102.
- (23) Kress, H.; Park, J.-G.; Mejean, C. O.; Forster, J. D.; Park, J.; Walse, S. S.; Zhang, Y.; Wu, D.; Weiner, O. D.; Fahmy, T. M.; Dufresne, E. R. *Nat. Methods* **2009**, *6*, 905–909.
- (24) King, K. R.; Wang, S.; Jayaraman, A.; Yarmush, M. L.; Toner, M. *Lab Chip* **2008**, *8*, 107–116.
- (25) Amarie, D.; Glazier, J. A.; Jacobson, S. C. *Anal. Chem.* **2007**, *79*, 9471–9477.
- (26) Leslie, D. C.; Easley, C. J.; Seker, E.; Karlinsey, J. M.; Utz, M.; Begley, M. R.; Landers, J. P. *Nat. Phys.* **2009**, *5*, 231–235.
- (27) Kuczenski, B.; Ruder, W. C.; Messner, W. C.; Leduc, P. R. *PLoS One* **2009**, *4*, e4847.
- (28) Unger, M. A. *Science* **2000**, *288*, 113–116.
- (29) Niu, X.; Gielen, F.; Edel, J. B.; DeMello, A. J. *Nat. Chem.* **2011**, *3*, 437–442.
- (30) Ahmed, D.; Mao, X.; Shi, J.; Juluri, B. K.; Huang, T. J. *Lab Chip* **2009**, *9*, 2738–2741.
- (31) Ahmed, D.; Mao, X.; Juluri, B. K.; Huang, T. J. *Microfluid. Nanofluid.* **2009**, *7*, 727–731.
- (32) Ahmed, D.; Chan, C. Y.; Lin, S.-C. S.; Muddana, H. S.; Nama, N.; Benkovic, S. J.; Huang, T. J. *Lab Chip* **2013**, *13*, 328–331.
- (33) Stroock, A. D.; Dertinger, S. K. W.; Ajdari, A.; Mezic, I.; Stone, H. A.; Whitesides, G. M. *Science* **2002**, *295*, 647–651.
- (34) Park, H. Y.; Qiu, X.; Rhoades, E.; Korlach, J.; Kwok, L. W.; Zipfel, W. R.; Webb, W. W.; Pollack, L. *Anal. Chem.* **2006**, *78*, 4465–4473.
- (35) Riahi, M.; Alizadeh, E. *J. Micromech. Microeng.* **2012**, *22*, 115001.
- (36) Harnett, C. K.; Templeton, J.; Dunphy-Guzman, K. a; Senousy, Y. M.; Kanouff, M. P. *Lab Chip* **2008**, *8*, 565–572.
- (37) Tsai, J.; Lin, L. *Sens. Actuators, A* **2002**, *97–98*, 665–671.
- (38) Hellman, A. N.; Rau, K. R.; Yoon, H. H.; Bae, S.; Palmer, J. F.; Phillips, K. S.; Allbritton, N. L.; Venugopalan, V. *Anal. Chem.* **2007**, *79*, 4484–4492.
- (39) Huang, P.-H.; Xie, Y.; Ahmed, D.; Rufo, J.; Nama, N.; Chen, Y.; Chan, C. Y.; Huang, T. J. *Lab Chip* **2013**, *13*, 3847–3852.
- (40) Ozcelik, A.; Ahmed, D.; Xie, Y.; Nama, N.; Qu, Z.; Nawaz, A. A.; Huang, T. J. *Anal. Chem.* **2014**, *86*, 5083–5088.
- (41) Lin, S.-C. S.; Mao, X.; Huang, T. J. *Lab Chip* **2012**, *12*, 2766–2770.
- (42) Ding, X.; Li, P.; Lin, S.-C. S.; Stratton, Z. S.; Nama, N.; Guo, F.; Slotcavage, D.; Mao, X.; Shi, J.; Costanzo, F.; Huang, T. J. *Lab Chip* **2013**, *13*, 3626–3649.
- (43) Ding, X.; Peng, Z.; Lin, S.-C. S.; Geri, M.; Li, S.; Li, P.; Chen, Y.; Dao, M.; Suresh, S.; Huang, T. J. *Proc. Natl. Acad. Sci. U.S.A.* **2014**, *111*, 12992–12997.
- (44) Hashmi, A.; Heiman, G.; Yu, G.; Lewis, M.; Kwon, H.-J.; Xu, J. *Microfluid. Nanofluid.* **2012**, *14*, 591–596.
- (45) Marmottant, P.; Hilgenfeldt, S. *Nature* **2003**, *423*, 153–156.
- (46) Tho, P.; Manasseh, R.; Ooi, A. J. *Fluid Mech.* **2007**, *576*, 191–233.
- (47) Leighton, T. G. *The Acoustic Bubble*; Academic Press: London, 1994; p 129.
- (48) Tovar, A. R.; Lee, A. P. *Lab Chip* **2009**, *9*, 41–43.
- (49) Xu, Y.; Hashmi, A.; Yu, G.; Lu, X.; Kwon, H.-J.; Chen, X.; Xu, J. *Appl. Phys. Lett.* **2013**, *102*, 023702.
- (50) Rogers, P.; Gralinski, I.; Galtry, C.; Neild, A. *Microfluid. Nanofluid.* **2012**, *14*, 469–477.
- (51) Lei, J.; Hill, M.; Glynne-Jones, P. *Lab Chip* **2014**, *14*, 532–541.
- (52) Barnkob, R.; Augustsson, P.; Laurell, T.; Bruus, H. *Phys. Rev. E* **2012**, *86*, 056307.
- (53) Ohlin, M.; Christakou, A. E.; Frisk, T.; Önfelt, B.; Wiklund, M. J. *Micromech. Microeng.* **2013**, *23*, 035008.
- (54) Dentry, M. B.; Yeo, L. Y.; Friend, J. R. *Phys. Rev. E* **2014**, *89*, 013203.
- (55) Song, H.; Ismagilov, R. F. *J. Am. Chem. Soc.* **2003**, *125*, 14613–14619.
- (56) Salmon, J.-B.; Dubrocq, C.; Tabeling, P.; Charier, S.; Alcor, D.; Jullien, L.; Ferrage, F. *Anal. Chem.* **2005**, *77*, 3417–3424.
- (57) Kholodenko, B. N.; Hancock, J. F.; Kolch, W. *Nat. Rev. Mol. Cell Biol.* **2010**, *11*, 414–426.
- (58) Dittrich, P. S.; Manz, A. *Nat. Rev. Drug Discovery* **2006**, *5*, 210–218.
- (59) Abate, A. R.; Hung, T.; Mary, P.; Agresti, J. J.; Weitz, D. A. *Proc. Natl. Acad. Sci. U.S.A.* **2010**, *107*, 19163–19166.
- (60) Reiter, E.; Ahn, S.; Shukla, A. K.; Lefkowitz, R. J. *Annu. Rev. Pharmacol. Toxicol.* **2012**, *52*, 179–197.
- (61) Luttrell, L. M.; Lefkowitz, R. J. *J. Cell. Sci.* **2002**, *115*, 455–465.
- (62) Böhme, I.; Beck-Sickinger, A. G. *Cell Commun. Signaling* **2009**, *7*, 16.
- (63) Kelly, E.; Bailey, C. P.; Henderson, G. *Br. J. Pharmacol.* **2008**, *153*, S379–S388.
- (64) Stickle, D.; Barber, R. *Biochem. Pharmacol.* **1991**, *42*, 1069–1077.
- (65) Ferguson, S. S. *Pharmacol. Rev.* **2001**, *53*, 1–24.
- (66) Krasel, C.; Büinemann, M.; Lorenz, K.; Lohse, M. J. *J. Biol. Chem.* **2005**, *280*, 9528–9535.
- (67) Goral, V.; Jin, Y.; Sun, H.; Ferrie, A. M.; Wu, Q.; Fang, Y. *PLoS One* **2011**, *6*, e19282.
- (68) Lohse, M. J.; Hein, P.; Hoffmann, C.; Nikolaev, V. O.; Vilardaga, J.-P.; Büinemann, M. *Br. J. Pharmacol.* **2008**, *153*, S125–S132.
- (69) Ding, X.; Lin, S.-C. S.; Kiraly, B.; Yue, H.; Li, S.; Shi, J.; Benkovic, S. J.; Huang, T. J. *Proc. Natl. Acad. Sci. U.S.A.* **2012**, *109*, 11105–11109.
- (70) Huang, P.-H.; Nama, N.; Mao, Z.; Li, P.; Rufo, J.; Chen, Y.; Xie, Y.; Wei, C.-H.; Wang, L.; Huang, T. J. *Lab Chip* **2014**, *14*, 4319–4323.
- (71) Li, S.; Guo, F.; Chen, Y.; Ding, X.; Li, P.; Wang, L.; Cameron, C. E.; Huang, T. J. *Anal. Chem.* **2014**, *86*, 9853–9859.
- (72) Ding, X.; Lin, S.-C. S.; Lapsley, M. I.; Li, S.; Guo, X.; Chan, C. Y.; Chiang, I. K.; McCoy, J. P.; Huang, T. J. *Lab Chip* **2012**, *12*, 4228–4231.
- (73) Le Gac, S.; van den Berg, A. *Trends Biotechnol.* **2010**, *28*, 55–62.